ELSEVIER

Nuclear Instruments and Methods in Physics Research A 399 (1997) 463–476

NUCLEAR INSTRUMENTS & METHODS IN PHYSICS RESEARCH Section A

Performances and characteristics of a prototype symmetric hybrid adjustable phase undulator

C.S. Hwang[a,b,*], C.H. Chang[a], T.C. Fan[a], F.Y. Lin[a], Ch. Wang[a], Shuting Yeh[a], H.P. Chang[a], K.T. Hsu[a], L.H. Chang[a], P.K. Tseng[a,c], T.M. Uen[b]

[a] *Synchrotron Radiation Research Center, Instrument Development Divisions, Hsinch Science-Based Industrial Park, 1 R&D Rd, VI Hsinchu, 30077, Taiwan*

[b] *Department of Electrophysics, National Chiao Tung University, Hsinchu, Taiwan*

[c] *Department of Physics, Tamkang University, Tamsui, Taiwan*

Received 31 January 1997; received in revised form 25 April 1997

Abstract

In this work, we construct and measure a prototype symmetric Hybrid Adjustable Phase Undulator (HAPU) with nine poles to compare phase change and gap change in terms of their features and performances. HAPU can also provide the different characteristics between the pure and hybrid adjustable phase undulator. The HAPU has been installed in the Synchrotron Radiation Research Center (SRRC) storage ring to test the performance of the beam dynamics and photon flux behavior. A three-orthogonal Hall probe and a long-loop-coil measurement system are also implemented to take the field measurements. The multipole field and electron trajectory correction are made by shimming, the magic finger, and the active end pole coil corrector.

After the field measurements, the vertical integral strength of HAPU is markedly smaller than that of the Hybrid Adjustable Gap Undulator (HAGU) and confirm that no obvious distinction arises between HAPU and HAGU in terms of the spectrum flux. The electron beam dynamic performance in the storage ring indicates that the vertical tune shift of HAPU is three times smaller than that of HAGU. Meanwhile, the energy dynamic tuning with the digital global feedback turned on, the photon position and flux in the bending chamber beam line is invariant. In addition, the injection efficiency remains unaffected at any phase position and the electron beam lifetime does not change when HAPU is in the dynamic tuning.

1. Introduction

For most insertion device magnets, the magnet gap is altered to vary the magnetic field. Such an undulator device is called the Adjustable Gap Undulator (AGU). A different design concept attempts to maintain a constant gap in which two rows of magnets are longitudinally moved with respect to each other so that the magnetic field can be varied [1–3]. This type of undulator device is called the Adjustable Phase Undulator (APU). This method, associated with a unique magnet array

* Corresponding author. Tel.: +886 35 783890/6106; fax: +886 35 783892; e-mail: cshwang@alpha1.srrc.gov.tw.

PII S0168-9002(97)00966-2

arrangement, can create an elliptical polarizing light [4–8]. The primary advantages of APU magnet over AGU magnet is that in the former, the vertical field integral, tune, and the beta function are independent of phase position [1–3]. Besides, the former method has a much simpler and reliable mechanical design and high-precision mechanical control than the latter. If the built-in dipole corrector is deemed necessary, then the corrector field strength is independent of the phase (note the corrector field strength of AGU relies on the gap change). Therefore, Carr [1, 2] designed and implemented the concept of a Pure Adjustable Phase Undulator (PAPU) with a pure conventional Halbach type. The PAPU, although fabricated and tested at SSRL [9], did not have the field measurements taken. Based on the above merits of PAPU, a previous work constructed a prototype symmetric Hybrid Adjustable Phase Undulator (HAPU) with 9 pole at SRRC to test the above features and performance. Although a previous investigator predicted only a slight difference in the field features between the HAPU and PAPU structure, knowing exactly what differences arise in the magnetic field features, the beam dynamic effect and the photon spectrum behavior is of interest. Such an interest is owing to that the hybrid magnet can obtain a higher magnetic field strength than the pure one; in addition, the peak field is less sensitive to variations in pure magnet's angle of magnetization [10, 11]. In the APU design, the phase change has a longitudinal force [12], as created by the change in longitudinal field. This force should be carefully handled to avert any mechanical errors that would induce the field error and, ultimately, destroy the spectrum quality.

The HAPU [13] is 9 poles of the hybrid magnet with NdFeB block and vanadum permandur pole. The period length is 10 cm and the peak field is 0.825 T at 28 mm gap. To compensate for the first integral and correct the electron trajectory, two steering coils are located at the up and down streams. Herein, two long-loop coils are used to compensate for the transverse earth field of vertical and horizontal components. Previously, two magic fingers [14] were used to modify the fringe field which induces the strong sextupole field and the other multipole strength. The magic fingers can also be used to correct the first integral strength. The physical length of this HAPU is 0.65 m. In that investigation, the magnet structure was mounted on a one meter long C-frame support structure in which the gap can be moved parallel or in-phase motion. The HAPU consists of a stationary upper jaw and a movable lower jaw that is mounted on two slides at the two rails. A stepper motor can longitudinally move the lower jaw by $\pm\lambda_u/2$; therefore, a phase change of $\pm\theta = \pm 2\pi\Delta z/\lambda_u$ produces the linear polarization light. Fig. 1 depicts the motion direction and the device geometry of this HAPU magnet. Here Δz denotes the displacement of the moving jaw with respect to the fixed jaw (i.e., different phase location) and λ_u represents period length. The phase change simultaneously varied the vertical field strength and creates the longitudinal field strength. Meanwhile, a phase shift $\Delta\theta$ exists in the vertical and longitudinal field, which is equal to be one half of the phase θ [1].

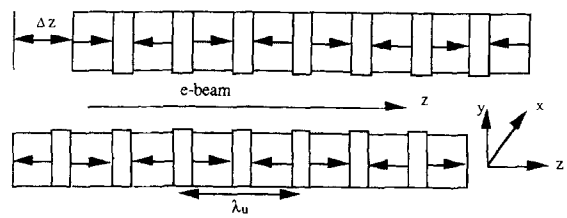

Fig. 1. The motion direction and the device geometry of this HAPU magnet. It shows the direction of easy axis of field in magnet blocks. Where Δz denotes zero for an AGU magnet.

This study also performs the field measurement by a three-orthogonal Hall probe with an automatic measurement stage which is "on the fly" method [15]. One probe is used for vertical field B_y measurement; the second one is used for the longitudinal field B_z; and the third one is used for the horizontal transverse field B_x measurement. The three Hall probe centers are not simultaneous at the same midplane and the Hall probe surface is not exactly perpendicular to each other. However, one method [15] can be used to adjust the relative center position and angle tilt between each Hall probe. After the adjustment, the relative position shift and the angle tilt are maintained within 0.15 mm and 0.2°. Finally, the relative position shift and the angle tilt are inserted into the analysis code

to compensate for the errors of the planar Hall effect as well as the position and angle error.

Herein, the field characteristics between the HAGU (gap motion) and HAPU (phase motion) is compared as well. Although the vertical field integral of the phase change has been changed 400 G cm, it is 600 G cm smaller than for the gap change (these results are constrained on the symmetry HAPU and no passive compensation is made). Hence, the HAPU is much less elaborate in constructing a dipole field corrector for the first integral strength compensation than the symmetry type of HAGU. In addition, several shims and two magic fingers are used to correct each pole's peak field, the vertical field integral and the multipole field. The vertical and longitudinal field simultaneously exist when changing the phase. If the phase is changed, the maximum vertical (longitudinal) field and minimum longitudinal (vertical) field occur at $\theta = 0$ ($\theta = \pm\pi$). Notably, the vertical peak field strength (at $\theta = 0$) is stronger than the longitudinal peak field strength (at $\theta = \pm\pi$) at a certain gap in this type of HAPU. Such peak field strength difference between the vertical and longitudinal field originate from differential magnetization in the iron pole. Therefore, the total field strength of $\sqrt{B_y^2 + B_z^2}$ decreases and becomes a flat line when the phase approaches $\theta = \pi$. This feature is in contrast with the pure-type PAPU (with the same magnet thickness and no magnet recess) which has a constant total field strength.

Field measurement results after the multipole and phase shimming (without any passive correction) of the hybrid structure indicate that the on-axis integrated field strength of the vertical components has been changed. However, this change of HAPU is markedly less than that of HAGU. In addition, the vertical integral field profile as a function of transverse x-axis also changed with a changing phase; but the change of the integral field profile is different from that of HAGU. Although the longitudinal field integral only changes slightly with a phase change, the multipole strength does not change. The ideal field with gap change and the field measurement with phase change are used to calculate the spectrum flux. The spectrum calculation results demonstrate that the photon spectrum output exponentially decays as a function of the optical rms phase error [16–19] and has the same tendency as HAGU. Therefore, the spectrum shimming is necessary to maintain a high spectrum intensity in different phase positions. However, because the prototype HAPU is an extremely short undulator, the photon flux of the real field calculation in the third harmonic is 2.5 times larger than the ideal field calculation.

Moreover, the HAPU is installed in the storage ring along with the performance and the features test as well. The injection efficiency remains unaffected when changing the phase from $\theta = 0$ to π. HAPU can be dynamically tuned without disturbing the other users in each beam line when the digital global feedback [20] is turned on. Notably, the tune shift induced from the vertical focusing strength [21] of the HAPU is three times smaller than the HAGU.

2. Field measurement and analysis

Magnetic field measurements were taken by moving a three-orthogonal Hall probe along the axis of the APU magnet, and recording the transverse components of vertical, horizontal, and the longitudinal field strength. 1200 measurements were taken at 1.2 mm interval for each Hall probe. When the gap was set to 28 mm the transverse field of vertical and horizontal components as well as the longitudinal field distribution were measured at various phases as Fig. 2 reveals. Fig. 2 indicates that the field distributions B_y and B_z along the longitudinal axis are sin-like waves. In addition, the two periodic fields of the two on-axis components are in-phase at any phase location. However, a phase shift $\Delta\theta = \theta/2$ (i.e., the location of the two peak field strength will be simultaneously shifted to be $\theta/2 = \pi\Delta z/\lambda_u$ when the phase was changed to the location of $\theta = 2\pi\Delta z/\lambda_u$) of the two periodic field is observed at a different phase θ location (see Fig. 2). The horizontal transverse field strength B_x is always extremely small. Meanwhile, the phase is fixed at zero and the gap is changed from 22 to 150 mm (in the AGU structure), the peak field strength exponentially varies with gap. The empirical formula Eq. (1) shows the field variation B_y of AGU and Eq. (2) presents the total field strength B_{AGU} in

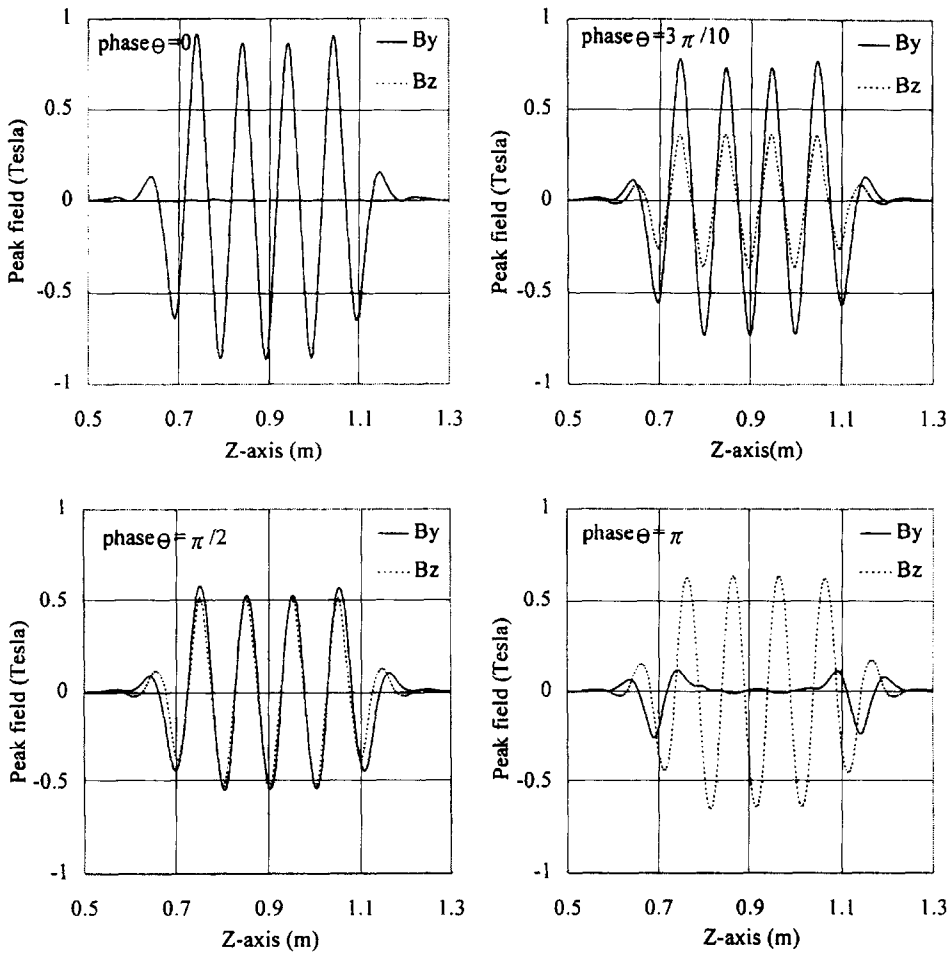

Fig. 2. Measurements of the peak field strengths B_y, B_z and B_x at 28 mm gap and phase $\theta = 0$, $\theta = 3\pi/10$, $\theta = \pi/2$ and $\theta = \pi$, respectively.

which the two components B_y and B_z are combined. Because the B_z is equal to zero, B_{AGU} is equal to $B_{y0}(g)$.

$$B_y = B_{y0}(g) = 3.44 \exp[(-g/\lambda_u)(5.08 - 1.54g/\lambda_u)], \tag{1}$$

$$B_{AGU} = \sqrt{B_y^2 + B_z^2} = B_{y0}(g), \tag{2}$$

where $0.085 < g/\lambda_u < 0.8$ and the field strength B_{AGU} exponentially vary as a function of gap and $B_{HAGU} = B_{PAGU} = B_{y0}(g)$. However, for the APU structure, the peak field of B_y and B_z are a slower, sinusoidal variation of field with longitudinal position which are shown in Eqs. (3) and (4) [1,2]. Eq. (5) shows the total field strength B_{APU} by combining the two components.

$$B_y = B_{y0}(g)\cos\theta, \tag{3}$$

$$B_z = F\,B_{y0}(g)\sin\theta, \tag{4}$$

$$B_{APU} = \sqrt{B_y^2 + B_z^2} = B_{y0}(g)\sqrt{1 + (F^2 - 1)\sin^2\theta}, \tag{5}$$

where θ denotes the phase change and $B_{y0}(g) = B_{AGU} = B_{APU}$ represents the vertical peak field

strength at phase location $\theta = 0$ and at certain magnet gap g, and F is function of the permeability and the geometry structure which include magnet array, location, and magnet thickness. In the PAPU geometrical structure similar to the Roger Carr design [1, 2], the magnet is of a material of unit permeability $\mu = 1$ and each magnet's thickness is the same and not any magnet recess occurs. Hence, $F = 1$ and $B_{\mathrm{PAPU}} = B_{y0}(g)$ are equal at each gap and phase (note the PAPU of Roger Carr structure has no magnet recess and has equal magnet thickness; if it is not this structure, then $F < 1$). Hence, B_{PAPU} is invariable with phase in this type of PAPU. However, for the hybrid structure of our type HAPU, the thickness of a magnet is different from that of a pole; in addition, HAPU has the magnet recess. Hence, F is a nonlinear function and smaller than 1. Therefore, the total field strength B_{HAPU} at a certain phase is less than $B_{y0}(g)$ and is varied as a phase. This nonequality of the peak field strength of B_{HAPU} and $B_{y0}(g)$ of HAPU should vanish with an increasing gap. Such an event is owing to that the nonequality peak-field originates from differential magnetization in the iron pole which derives from the permeability μ and the magnet array structure (the pure structure relies only on the magnet array structure). Fig. 3 presents the peak field strengths B_y and B_z as a function of phase measured at two different gaps. As this figure reveals, the total field strength B_{HAPU} and B_{HAGU} at two gaps of 22 and 28 mm are calculated according to field measurement results. The higher field strength of B_{y0} ($g = 22$ mm) has a stronger differential magnetization in iron pole such that the slope of the normalization curve $B_{\mathrm{HAPU}}/B_{y0}(g)$ become larger than the lower field strength of B_{y0} ($g = 28$ mm).

A situation is considered in which APU's magnetic field strength must be changed to obtain the exact deflection parameter K to fulfill the different photon energies. The vertical field strength is altered by changing the phase to obtain the K value that, subsequently, determines the photon energy. Under the same condition (i.e., the rms deviation of each block easy-axis magnetization field is 3% and the rms tilt-angle deviation is 2°. HAPU is without any field correction and shimming as well as magnet sorting), the vertical field integral

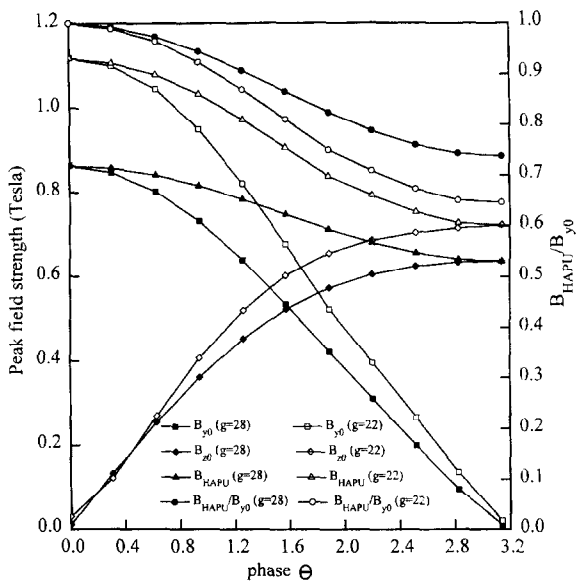

Fig. 3. Measurement and calculations of the field strengths B_y, B_z, and the total field strength B_{HAPU} and B_{HAGU} at two different gaps of 22 and 28 mm which have the different field strengths $B_{y0}(g)$. The change in phase among these this two gaps to display the relationship between peak field strength and phase.

strength between the gap change and phase change has been depicted in Figs. 4(a) and (b). Fig. 4(a) indicates, when changing the gap, the vertical integral field strength on-axis gradually decreases and the higher multipole strength also decreases. Such a behavior originates from the strong fringe field change of the end pole. However, some passive end pole corrector methods [22, 23] have recently been developed to overcome the fringe field change and maintained a small variation of field integral strength (within 50 G cm) when the gap is changed. Fig. 4(b) reveals that when changing the phase, the vertical field integral strength on-axis only slightly changes and the integral field profile apparently has the same behavior. This behavior reveals that the vertical field integral is less dependent of the fringe field when the phase changes. Fig. 4 shows that the vertical integral strength of HAGU is changed by 1000 G cm, but the HAPU is only changed by 400 G cm. Therefore, only a slight dipole correction must be made on the symmetric hybrid structure HAPU with no passive end pole corrector skill.

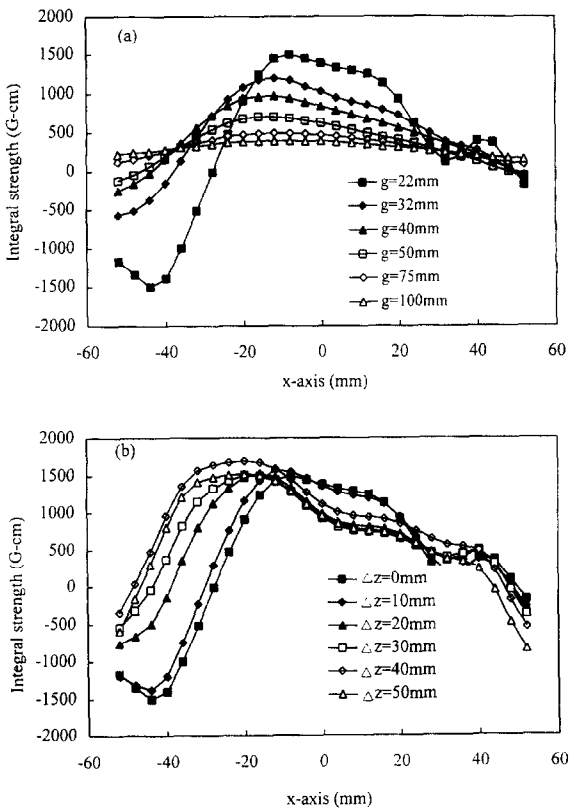

Fig. 4. (a) The profile of vertical field integral strength as a function of horizontal transverse axis when the gap was changed. This figure shows the multipole field behavior is varied at different gaps. (b) The profile of vertical field integral strength as a function of horizontal transverse axis when the phase was changed. This figure also displays the multipole field behavior is varied as different phase.

After the multipole shimming are used to correct the multipole field, Figs. 5 and 6 depict each harmonic integral strength as a function of phase which are analyzed in the range of $-30 \leq x \leq 30$ mm. Fig. 5 indicates the normal dipole integral strength (D_n) and skew dipole integral strength (D_s) simultaneously decrease when the phase changes. The normal dipole integral strength change of 400 G cm can be compensated for by the active end coil corrector. The skew dipole integral strength of 200 G cm can be corrected by mounting the long coils in fixed locations with 45° orientation with respect to the e-beam. This figure also reveals that when the phase is changed, the integral quadrupole strength (Q) remains constant at 100 G despite an increasing integral normal quadrupole strength (Q_n) and a decreasing skew quadrupole strength (Q_s), where the integral quadrupole strength is defined as $Q = \sqrt{Q_n^2 + Q_s^2}$. The integral quadrupole strength Q is only slightly beyond the specification requirements (the specification is 100 G). Herein, after the end pole coil corrector is excited, the first integral strength is corrected from 450 G cm to be zero and within the specification (the specification is 100 G cm). According to Fig. 6, the sextupole and octupole strength are changed in the phase change, but nearly within the specification (note the specification is 150 G/cm and 100 G/cm^2). However, the longitudinal harmonic integral strength are maintained constant, except the dipole field strength when the phase is changed. Fig. 7 displays the profile of the longitudinal field integral field strength as a different phase. Notably, the longitudinal dipole integral field strength on-axis changes about 170 G cm when the phase is changed from 0 to π.

3. Electron beam accelerator analysis

For the pure structure of PAPU, the tune shift and beta beating should be zero when the phase is changed. However, to what extent do tune shift and beta beating occur in the Hybrid structure of HAPU? Hence, for measuring the tune and beta function of HAPU, we fix the gap at 28 mm, for a maximum K of 7.85, when we vary the phase from 0 to π. Fig. 2 presents the vertical and longitudinal field variation. Meanwhile, the longitudinal field induces a periodic motion of the electron beam in the vertical direction. Fig. 8 depicts the electron trajectories projected on the x–y plane induced from the vertical B_y field and longitudinal B_z field for various phases. As this figure reveals, the vertical motion is markedly smaller than the horizontal motion. This behavior is owing to the fact that the transverse horizontal velocity is significantly smaller than the longitudinal direction, by a factor of $mc^2/E = 1/2549$ (for 1.3 GeV storage ring energy at SRRC). Therefore, in spite of the strong longitudinal field strength, the vertical oscillation neglects the effect on the emittance of the electron beam [1–3].

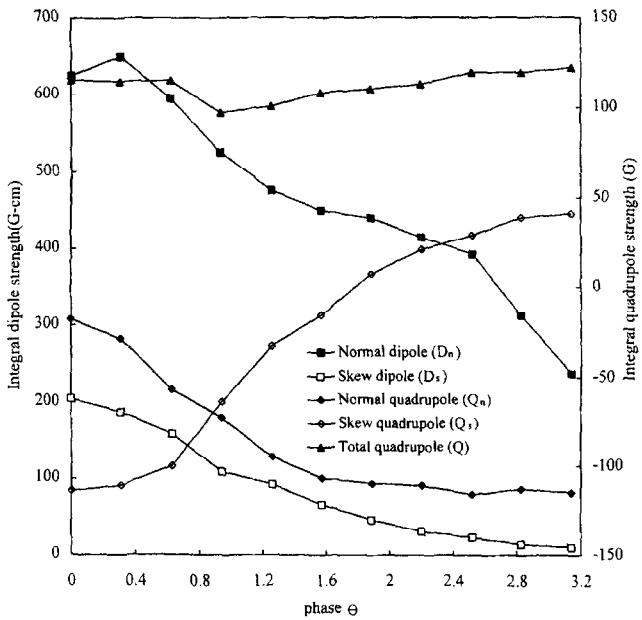

Fig. 5. Normal and skew terms of the dipole and quadrupole integral strength distribution in the different phases. The total quadrupole integral strength $Q = \sqrt{Q_n^2 + Q_s^2}$ is independent of phase.

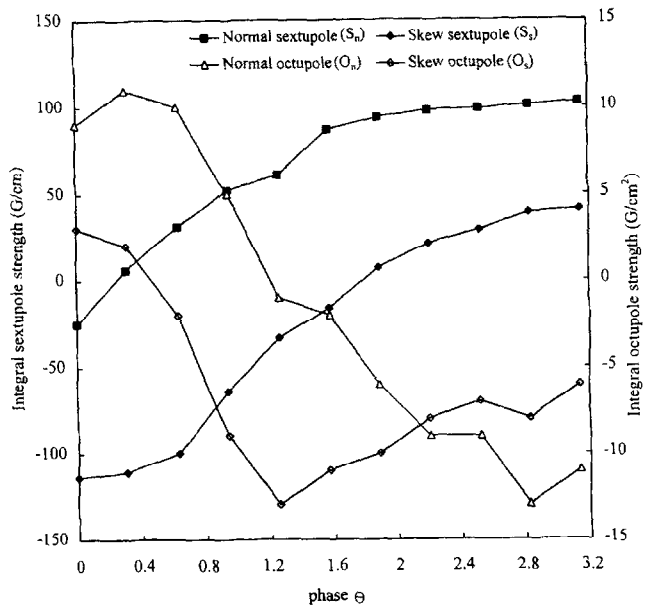

Fig. 6. Normal and skew terms of the sextupole and octupole integral strength distribution in the different phases.

For the APU or AGU, the field behavior resembles a drift space in the horizontal plane; hence, the horizontal tune shift is zero. However, there is an intrinsic focusing quadrupole strength in the vertical plane. The vertical focusing strength is a second-order effect which is proportional to the square of the field and inversely proportional to the square of the energy. According to the vertical focusing

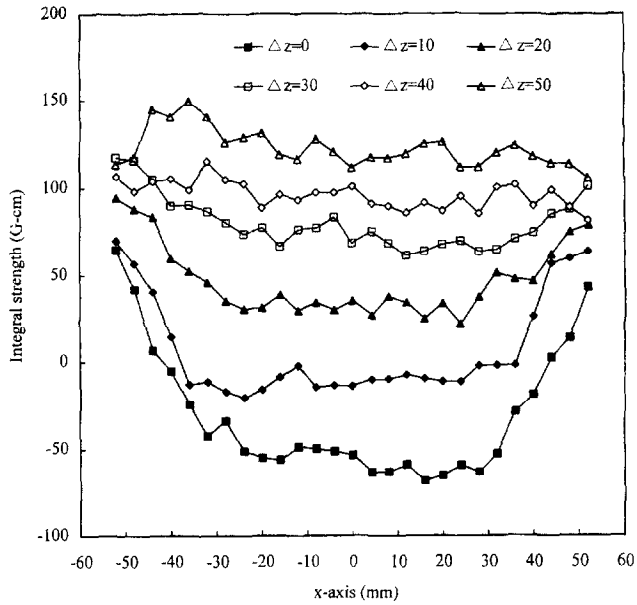

Fig. 7. Profile of the longitudinal field integral strength as different phase.

strength k_y which can be seen on the off-axis vertically, a longitudinal B_z field component couples to the angular deflection in the horizontal plane to produce a force which always acts towards the beam axis [21]. The equations of motion in the y–z plane in APU and AGU are described as [1, 21]

$$\frac{d^2y}{dz^2} = -\frac{1}{2}\left(\frac{eB_{\mathrm{HAPU}}}{E}\right)^2 y = -k_y y, \tag{6}$$

$$\frac{d^2y}{dz^2} = -\frac{1}{2}\left(\frac{eB_{\mathrm{HAGU}}}{E}\right)^2 y = -k_y y, \tag{7}$$

where E denotes the electron energy. The vertical tune shift ΔQ_y and the beta beating $\Delta\beta_y$ depend on the vertical focusing strength k_y and the magnet length L. Hence, the vertical tune shift and the beta beating can be expressed as [18]

$$\Delta Q_y = \frac{k_y\beta_y L}{4\pi}\left(1 + \frac{L^2}{12\beta_y^2}\right), \tag{8}$$

$$\Delta\beta_y = \frac{k_y\beta_y^2 L}{2\sin\mu}\left(1 - \frac{L^2}{12\beta_y^2}\right), \tag{9}$$

where β_y represents the vertical beta function and μ is the one-turn phase advance in the absence of the HAPU. Therefore, according to Eqs. (6)–(9), the vertical tune shift ΔQ_y relies on the field strength B_{HAPU} and the insertion device length L of the HAPU magnet. The vertical focusing strength k_y and the field strength B_{HAGU} of the HAGU magnet have a strong exponential change with gap. However, the field strength B_{HAPU} of HAPU magnet changes only slightly with the phase. Such a slight change is owing to the fact that the magnetization in the iron pole is a function of phase, although, the magnet gap g and periodic length λ_u is fixed. Fig. 9 presents the tune shift measurement and the field strength measurement of B_{HAGU} and B_{HAPU}. Also, included in this figure is the theoretical calculation of vertical tune shift of HAPU and HAGU. This figure confirms that the vertical tune shift of the HAPU is 3 times smaller than that of HAGU which corresponds to the field strengths square of B^2_{HAGU} and B^2_{HAPU}. Interestingly, the tune shift measurement is nearly the same as the theoretical calculation prediction. Based on Eqs. (8) and (9), the beta beating should be zero in the symmetry array of PAPU and

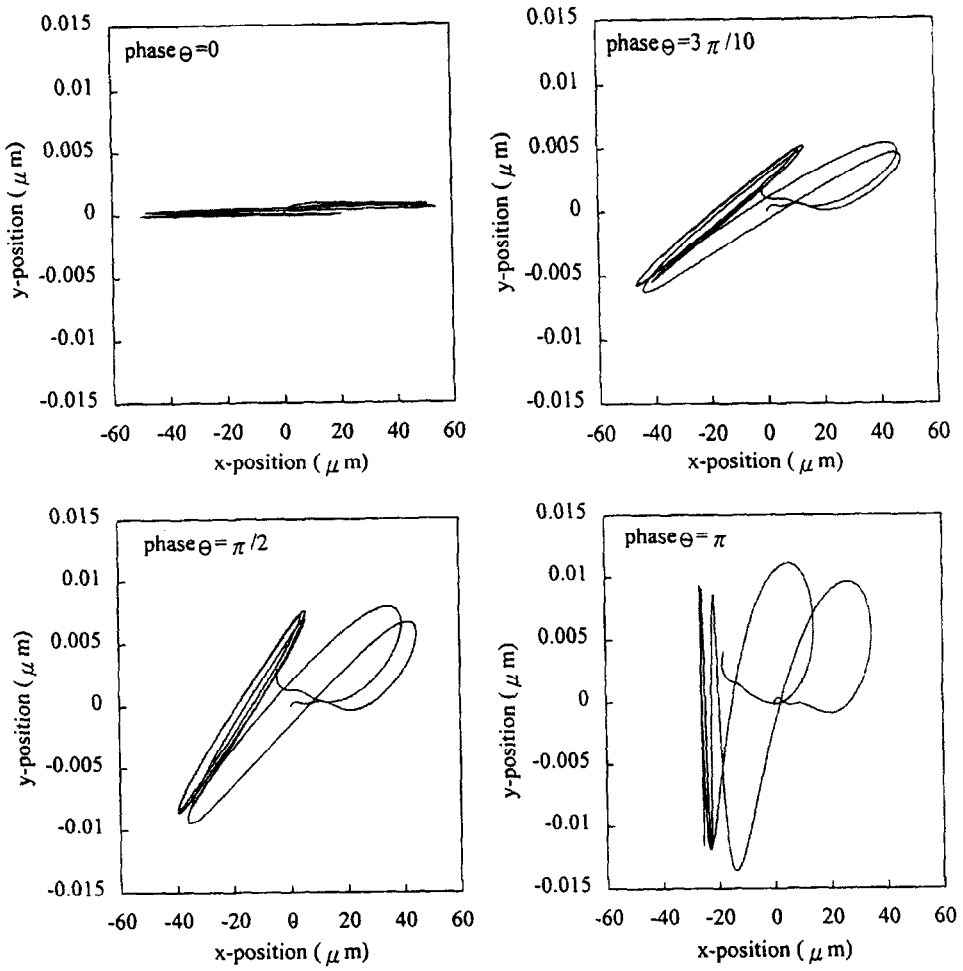

Fig. 8. Electron trajectories calculation from the field measurement as projected on the $x-y$ plane for various phases $\theta = 0$, $\theta = 3\pi/10$, $\theta = \pi/2$ and $\theta = \pi$ at 28 mm gap. The electron trajectories induced from the vertical and longitudinal field strength (at 1.3 GeV).

extremely small in HAPU magnet. The above results demonstrate that HAPU has a positive performance in the tune shift and beta beating.

The electron beam close orbit has a 20 μm variations in horizontal and vertical planes on the dynamic energy tuning and the photon intensity has been changed about 6% (see Fig. 10). However, when the digital global feedback system [20] is turned on, the electron beam trajectory has been corrected to the same close orbit, thereby not changing the photon flux and not influencing the users when the HAPU is in the dynamic tuning mode. The beam lifetime also remains unaffected in the dynamic tuning mode when the global feedback system is turned on\off. Fig. 10 displays the photon beam behavior in the beam line. Two photon beam position monitors are located at different positions on the bending magnet beam line. According to this figure, the photon flux has changed 6% when the phase is changed. However, when the global feedback is tuned on, the photon position remains constant in the two photon beam position monitor. When the global feedback is again tuned on at the duration of 1035–1100 s, the photon position returns to the same position; the photon flux also returns to the same flux as well. The above

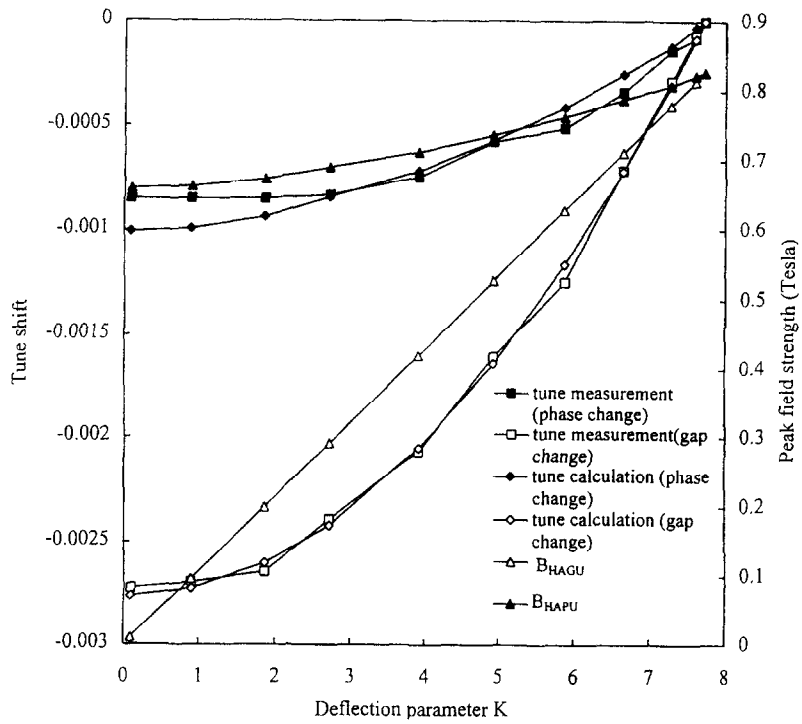

Fig. 9. Vertical-tune-shift comparison between the phase change and gap change in the measurement and theoretical calculation. The total field strength of B_{HAPU} and B_{HAGU} at gap change and phase change are correlated with the vertical tune shift.

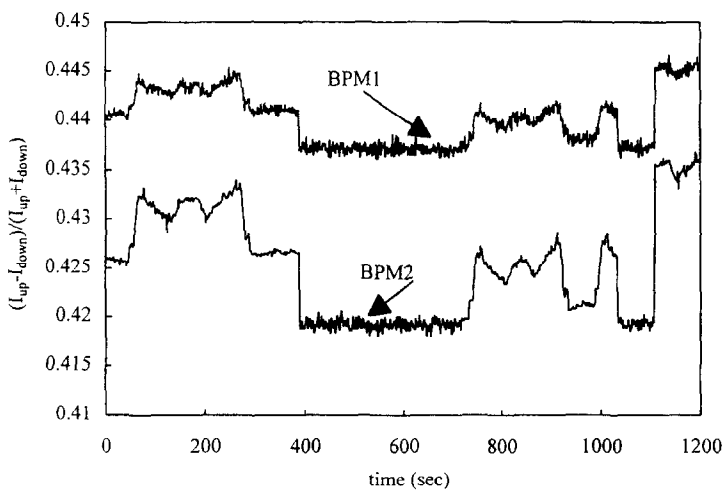

Fig. 10. The photon position behavior on the bending magnet beam line. From the time duration ranging from 0 to 380 s, the HAPU moved from phase $\theta = 0$ to $\theta = \pi$ and then return to $\theta = 0$ (The time duration of the global feedback turned off). When the time duration ranges from 380 to 730 s, the HAPU also moved from phase $\theta = 0$ to $\theta = \pi$ and then returned to $\theta = 0$. However, the global feedback turned on. Between 730 and 1035 s, the corrector pulse current of the global feedback system turned off. Between 1035 and 1100 s, the global feedback turned on again.

results demonstrate that turning on the global feedback the electron trajectory was kept in the same close orbit and, hence, does not affect the user in the other beamline.

4. Photon spectrum analysis

Because there is no net horizontal field ($B_x \ll B_y$) in the type of HAPU, there is only linear polarization in the horizontal plane. For the spectrum quality control, the spectrum shimming is performed and the field measurement results are inserted into the spectrum phase calculation. The spectrum phase calculation relies on the equation for the energy radiation phase $\Theta(t)$ as defined in Eqs. (10) and (11) [16–19].

$$\frac{\mathrm{d}^2 I}{\mathrm{d}\omega\,\mathrm{d}\Omega} = \frac{e^2\omega^2 Z_0}{16\pi^3}\left(\int_{-\infty}^{\infty} \boldsymbol{n}\times(\boldsymbol{n}\times\beta)^{\mathrm{i}\omega\Theta(t)}\,\mathrm{d}t\right)^2, \tag{10}$$

$$\Theta(t) = \omega\left(t - \frac{\boldsymbol{n}\cdot\boldsymbol{r}(t)}{c}\right), \tag{11}$$

where e denotes the electronic charge, Z_0 represents the impedance of free space, $\boldsymbol{n}$ is the unit vector, $\beta = v/c$ and $\boldsymbol{r}(t)$ denotes the electron velocity and position vector. On-axis, the radiation phase of the relativistic electron depends on the first integral strength at each pole's location. Therefore, Eq. (11) can be written as

$$\Theta(z) = \frac{2\pi}{\lambda}\left(\frac{z}{2\gamma^2} - \frac{\int x'^2\,\mathrm{d}z}{2}\right). \tag{12}$$

where $x' = \mathrm{d}x/\mathrm{d}z$ represents the electron angle with respect to the undulator z-axis, λ is the photon radiation fundamental wavelength, and γ denotes the relativistic velocity. In the ideal undulator device, the phase at each pole should be a perfect linear variation and the phase error is zero. However, for a real undulator, the phase error $\Delta\Theta$ is not zero and can be obtained by subtracting the two optimum linear fits of the real and ideal field (which can be obtained from the real-field sinusoidal best fit) from the phase calculation of Eq. (12). Fig. 11 depicts the spectrum rms phase error $\Delta\Theta_{\mathrm{rms}}$ as a function of phase. This figure also displays the relation between the harmonic energy photon flux and the rms phase error $\Delta\Theta_{\mathrm{rms}}$ in the different deflection parameter K. Where $K = 0.934\ B_y\lambda_u$, and λ_u represents the periodic length. The photon emission of each harmonic energy E_n can be calculated by Eq. (13) which is expressed as

$$E_n(\mathrm{KeV}) = \frac{n0.95E_e^2(\mathrm{GeV})}{\lambda_u(\mathrm{cm})(1 + K^2/2 + \gamma^2\theta^2)}. \tag{13}$$

where n is the odd harmonic spectrum numbers, θ denotes the angle between the electron source and the observer, and $E_e = \gamma mc^2$ represents the relative energy of the electrons. For the spectrum calculation of the real-field measurement and the ideal field of HAPU, we fix the gap at 28 mm, for a maximum K of 7.85 and then vary the phase from 0 to π. Fig. 11 depicts the first to fifth harmonic spectrum flux normalized to the ideal flux. The ideal spectrum flux is calculated from the ideal field strength with different gap (HAGU); the real spectrum is calculated from the field measurement with different phase (HAPU). As this figure implies, in terms of the spectrum, there is almost the same results between HAGU and HAPU. In addition, the harmonic spectrum of these two methods have the same tendency. This same figure also reveals that when the phase is at zero ($k = 7.85$), the third harmonic flux of the real field is 2.5 times larger than the ideal field; the first and fifth harmonic spectrum are also slightly larger than the ideal field. Such a behavior is due to the end pole effect. Fig. 12 reveals that different numbers of center pole contribute different fluxes in the first to fifth harmonic spectrum. As clearly demonstrated in this figure, the end poles effect is typical of a device having a short length. Also observed in this figure is that the third harmonics of the real-field measurement is not only higher but narrower (because the relative bandwidth at the nth harmonic is $\Delta\omega/\omega \cong 1/nN$, where N denotes the number of periods) than that of the ideal undulator. However, the narrower spectrum is broadened when extracting the end pole. Notably, interference effects arise from the extremity that may enhance and/or compress some harmonics. Hence, a different peak field strength in some pole with a periodic sinusoidal field can be designed to enhance or compress the harmonic spectrum. Fig. 11 also presents the predicted results of the each harmonic flux intensity I and rms

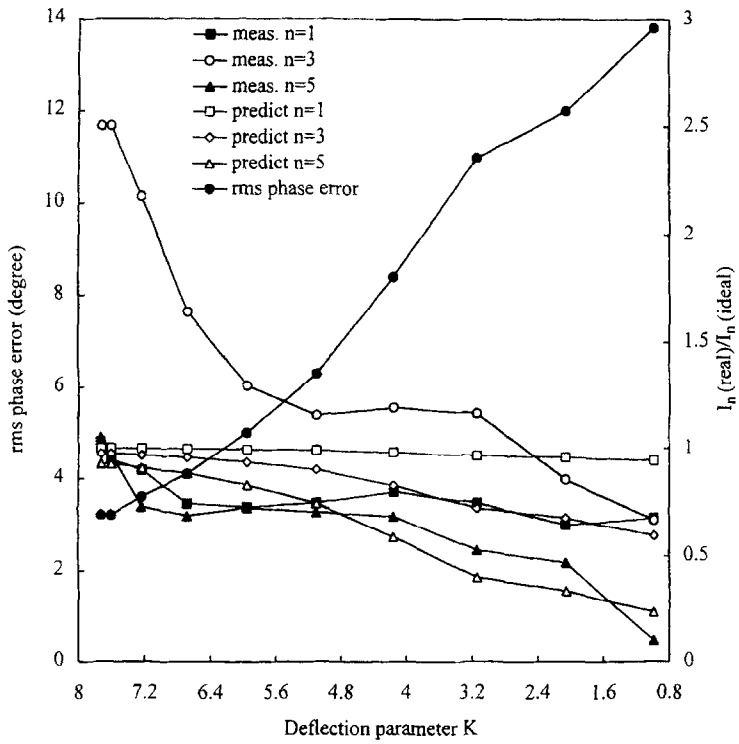

Fig. 11. Photon flux normalization between the field measurement results and the ideal field calculation as a function of deflection parameter K. This figure also predicts the relation between the rms phase error $\Delta\Theta_{rms}$ and the photon flux density variation.

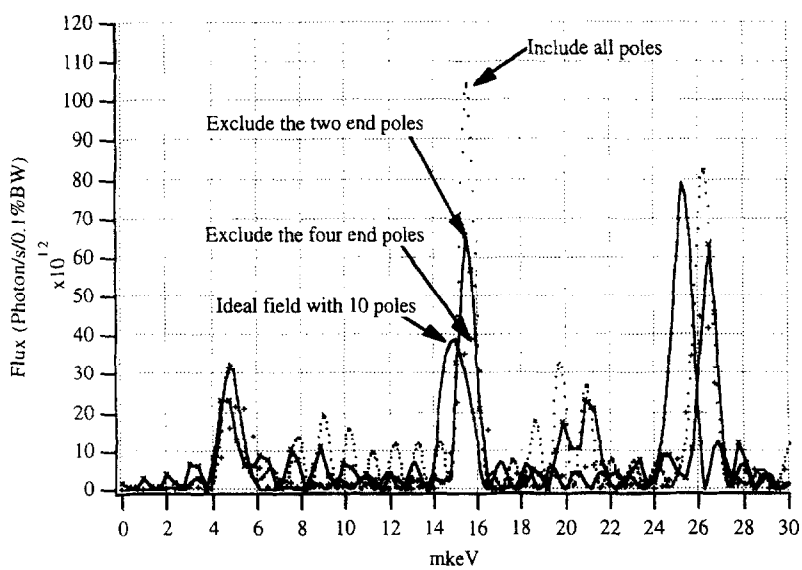

Fig. 12. The field measurement results in the different number of center poles which are 7, 9 and 11 individually. The photon flux calculation of the field measurement results are compared with the total flux of the ideal ten-pole field spectrum calculation.

phase error $\Delta\Theta_{\rm rms}$ when the phase changes. A correlation arises between the flux intensity I and rms phase error $\Delta\Theta_{rms}$, which can be used a figure-of-merit in designing the undulator. Eq. (14) shows the empirical formula between spectrum flux and phase error.

$$I = I_0 e^{-(n\Delta\Theta_{\rm rms})^2}, \tag{14}$$

where I and I_0 represent the spectrum flux intensities with and without phase error. Although relative intensities of the harmonics vary according to the empirical formula Eq. (14), but due to too few poles in this prototype HAPU, the statistic number is insufficient to exhibit the quantity. Therefore, the relative intensities of the harmonics of this 9 pole HAPU (the two end poles have been excluded) have the same tendency with the rms phase error, but not the same quantity.

5. Conclusions

Among the merits of this type of HAPU presented herein include (a) the simple drive train and reliable mechanical accuracy control, (b) the tune shift and beta beating are smaller than the HAGU, and (c) only a slight change in first integral strength occurs when the phase is changed. Hence, less dipole field strength correction is necessary in this kind of symmetry structure and nonpassive end correction HAPU magnet. Although the higher multipole strengths are also changed when the phase is changed, the higher harmonic integral strengths are all maintained within or close to the specification.

Notably, the field strength of $B_{\rm HAPU}$ is slightly varied as the phase. This is due to the opposite polarity magnetic flux which will decrease the magnetization strength on the iron poles when the phase was changed. Meanwhile, the field strength has no field superposition features in HAPU. Hence, the tune shift will be larger than the symmetry array of PAPU magnet. Therefore, the hybrid structure is less appropriate for designing the elliptical polarization undulator than the pure structure despite that (a) the hybrid structure can yield a higher magnetic field strength, and (b) the roll-off and field variation of peak field are less sensitive to the variation and inhomogeneity field of the pure magnet.

Although no beam line is available to test the spectrum quality, the field measurement data in different phase has been inserted into the spectrum calculation. The spectrum calculation in different phases is similar to the actual field spectrum calculation in different gaps. Therefore, spectrum analysis results demonstrate that the HAPU and HAGU have no obviously different spectrum behavior. According to Fig. 12, a different peak field strength can be designed on a certain pole (fixed the periodic length) [24] to compress some harmonic spectrum and enhance the harmonic spectrum we want. In addition, in the APU, although the strong longitudinal field strength has been created when the phase is changed, the transverse velocity is too small to affect the electron trajectory and the photon spectrum.

Acknowledgments

The authors are indebted to Dr. Roger Carr (SSRL) for valuable discussions regarding the field analysis. Dr. Pascal Elleume (ESRF) is also appreciated for his comments regarding the spectrum and field measurement analysis and his user friendly B2E program. The authors are indebted to Director Y.C. Liu (SRRC), Deputy Director C.T. Chen (SRRC), Dr. J.R. Chen (SRRC) to support this project. SRRC staff members J.Y. Hsu, H.H. Chen and K.H. Chen are also commended for their technical assistance.

References

[1] Roger Carr, Heinz-Dieter Nuhn, Rev. Sci. Instrum. 63 (1) (1992).
[2] Roger Carr, Nucl. Instr. and Meth. A 306(1991) 391.
[3] Steve Lidia, Roger Carr, Nucl. Instr. and Meth. A 347 (1994) 77.
[4] Pascal Elleaume, Nucl. Instr. and Meth. A 291(1990) 371.
[5] Shigemi Sasaki, Koji Miyata, Takeo Takada, Jpn. J. Appl. Phys. 31 (1992) 1794.
[6] Shigemi Sasaki, Nucl. Instr. and Meth. A 347(1994) 83.
[7] Roger Carr, Int. Conf. on High Energy Accelerators, 1993, p. 1596.
[8] Richard P. Walker, European Particle Accelerator Conference (EPAC'92), 1992, p. 310.
[9] Roger Carr, Heinz-Dieter Nuhn, and Jeff Corbett, European Particle Accelerator Conf. (EPAC'92), 1992, p. 489.

[10] Klaus Halback, J. Appl. Phys. 57 (1) (1985) 3605.
[11] R.P. Walker, Nucl. Instr. and Meth. A 237(1985) 366.
[12] Ch. Wang et al., European Particle Accelerator Conf. (EPAC'96), Barcelona, Spain, 10–14 June 1996.
[13] C.H. Chang, L.H. Chang, H.H. Chen, T.C. Fan, C.S. Hwang, D.L. Kuo, J.Y. Hsu, F.Y. Lin, Ch. Wang, Shuting Yeh, IEEE Trans. Magn. 32 (4) (1996) 2629.
[14] E. Hoyer, S. Mark, P. Pipersky, R. Schlueter, Rev. Sci. Instrum. 66 (2) (1995).
[15] C.S. Hwang, T.C. Fan, F.Y. Lin, Shuting Yeh, C.C. Chen, C.H. Chang, SRRC/MG/ IM/97-01.
[16] Bruno Diviacco, Richard P. Walker, Nucl. Instr. and Meth. A 368 (1996) 522.
[17] B.L. Bobbs, G. Rakowsky, P. Kennedy, R.A. Cover, D. Slater, Nucl. Instr. and Meth. A 296 (1990) 574.
[18] Roger J. Dejus, Isaac Vasserman, Elizabeth R. Moog, and Efim Gluskin, Rev. Sci. Instrum. 66 (2) (1995) 1875.
[19] B.M. Kincaid, J. Opt. Soc. Am. B 2 (1985) 1294.
[20] C.H. Kuo et al., European Particle Accelerator Conf. (EPAC'96), Barcelona, Spain, 10–14 June 1996.
[21] S. Tunner, Cern accelerator school fifth advanced accelerator physics course (CAS), vol. II, CERN 95-06, 1995, p. 807.
[22] I. Vasserman, E.R. Moog, Rev. Sci. Instrum. 66 (2) (1995) 1943.
[23] J. Pfluger, Rev. Sci. Instrum. 63 295 (1992).
[24] Shinya Hashimoto, Shigemi Sasaki, Nucl. Instr. and Meth. A 361 (1995) 611.
[25] C.S. Hwang et al., European Particle Accelerator Conf. (EPAC'96), Barcelona, Spain, 10–14 June 1996.